Extracting the asymptotic normalization coefficient for the $^{14}C \rightarrow {}^{13}B + p$ overlap from the $^{14}C(^{11}B, {}^{12}C)\,{}^{13}B$ reaction

S. Yu. Mezhevych,[1] N. Keeley,[2,*] A. T. Rudchik,[1] K. Rusek,[3] K. W. Kemper,[4] A. A. Rudchik,[1] O. A. Ponkratenko,[1] E. I. Koshchy,[5] and S. B. Sakuta[6]

[1]*Institute for Nuclear Research, Ukrainian Academy of Sciences, Prospect Nauki 47, 03680 Kyiv, Ukraine*
[2]*National Centre for Nuclear Research, ul. Andrzeja Sołtana 7, PL-05-400 Otwock, Poland*
[3]*Heavy Ion Laboratory, University of Warsaw, Pasteura 5A, PL-02-093 Warsaw, Poland*
[4]*Department of Physics, Florida State University, Tallahassee, Florida 32306, USA*
[5]*Cyclotron Institute Texas A&M University, College Station, Texas 77843, USA*
[6]*Russian Research Center "Kurchatov Institute", Kurchatov Square 1, 123182 Moscow, Russia*

(Received 31 December 2021; accepted 17 February 2022; published 24 February 2022)

The availability of a comparatively complete data set for the elastic and inelastic scattering of a 45-MeV beam of ^{11}B ions from a ^{14}C target, together with an angular distribution for the $^{14}C(^{11}B, {}^{12}C)\,{}^{13}B$ proton pickup reaction enables a determination of the $\langle {}^{14}C \mid {}^{13}B + p\rangle$ asymptotic normalization coefficient (ANC) using the coupled reaction channel (CRC) technique. The complete nature of the data set allows two-step contributions to the reaction mechanism to be controlled while a set of $\langle {}^{12}C \mid {}^{11}B + p\rangle$ overlaps obtained from a consistent analysis of $(d, {}^{3}He)$ and $(e, e'p)$ data fixes the projectile overlaps. We find that the level of completeness of the modeling of the reaction mechanism has a significant effect on the value obtained for the ANC, with a distorted wave Born approximation analysis yielding a significantly larger ANC than the full CRC calculation. The final result obtained, when compared with the theoretical value calculated within the source term approach, is in accord with trends for proton removal from similar p-shell nuclei.

DOI: 10.1103/PhysRevC.105.024615

I. INTRODUCTION

It has long been recognized that the extraction of absolute spectroscopic factors from direct reaction data is bedeviled by the sensitivity of the values obtained to the choice of the parameters of the potential binding the transferred particle to the core nucleus. If the usual well-depth prescription is adopted, together with a Woods-Saxon binding potential, the spectroscopic factor can vary by factors of two or more over a reasonable range of values for the radius parameter (the sensitivity to the choice of the diffuseness is much less marked). This problem may, however, be obviated if the rms radius of the bound-state radial wave function can be fixed by other means, for example, analysis of $(e, e'p)$ measurements in the case of proton transfer. Notwithstanding, such data are not always available, and while structure calculations may be used instead it can be difficult to assess accurately the contribution to the overall uncertainty in the extracted spectroscopic factor of such usage. Also, there remains the problem that spectroscopic factors for the same overlaps extracted using different binding potential radius values cannot be meaningfully compared.

To facilitate comparison of structure information extracted from direct reaction data the reduced normalization Λ was introduced [1–3] in the 1960s for neutron transfer reactions as a quantity that is nearly independent of binding potential geometry. The reduced normalization $\Lambda_{\ell j}$ is defined as the asymptotic normalization of the bound-state neutron wave function $u_{\ell j}(r)$ [4]:

$$u_{\ell j}(r) = \langle B \mid A\rangle = [(2J_B + 1)\Lambda_{\ell j}]^{1/2} k_B^{3/2} i^{-1} h_\ell^1(ik_B r), \quad (1)$$

valid for large radii r and where $E_B = (\hbar k_B)^2/2\mu_n$ and μ_n denote the binding energy and reduced mass of the neutron in the $B = A + n$ system, respectively, and h_ℓ^1 is a spherical Hankel function of the first kind. For practical use in standard distorted wave Born approximation (DWBA) codes $\Lambda_{\ell j}$ is related to the usual spectroscopic factor $S_{\ell j}$:

$$\Lambda_{\ell j} = S_{\ell j}\Lambda_{\ell j}^{\rm sp}, \quad (2)$$

with $\Lambda_{\ell j}^{\rm sp}$ calculated using Eq. (1) with $u_{\ell j}(r)$ taken to be the wave function $u_{\ell j}^{\rm sp}(r)$ of a single neutron bound in a Woods-Saxon well with binding energy E_B. In a similar vein the asymptotic normalization coefficient (ANC) was introduced some years later [5,6]. It is conceptually identical with the reduced normalization, although there are differences of detail. For use in standard DWBA codes the ANC $C_{\ell j}$ is related to the spectroscopic factor in the following way [7]:

$$C_{\ell j}^2 = S b_{\ell j}^2, \quad (3)$$

*Corresponding author:nicholas.keeley@ncbj.gov.pl

where b is the "single particle" ANC which may be obtained from the following relation [7]:

$$u_{\ell j}(r) = b_{\ell j}\frac{W_{-\eta,\ell+1/2}(2k_B r)}{r}, \tag{4}$$

again valid for large r and where $\eta = Z_n Z_A e^2 \mu_n/(\hbar^2 k_B)$ is the Coulomb parameter of the $B = A + n$ system (note that n need not be a neutron in this case but may be a proton or α particle, for example) and W is a Whittaker function of the second kind. The reduced normalization was initially developed for neutron transfer overlaps only and has seen little or no application to charged particle transfers, while the ANC is routinely used for both. However, for transfers of charged particles involving weakly bound levels the ANC can become inconveniently large, so that a Coulomb renormalized ANC was introduced [8] for use in these circumstances.

The applicability of both the reduced normalization and the ANC rests on the requirement that the reaction is sensitive only to the tail of the radial wave function of the transferred particle. In the case of the reduced normalization this is usually ensured through the use of sub- or near-Coulomb barrier reactions which involves experimental difficulties associated with small cross sections and sensitivity to target contaminants. The shapes of the sub-Coulomb transfer angular distributions are also essentially insensitive to the transferred angular momentum, meaning that they can only be applied to levels where the spin parity is already known. For ANCs it was found that for incident energies up to about 10 MeV/nucleon the reaction is still sufficiently peripheral even for most light-ion projectiles. It should be noted that both the reduced normalization and the ANC, while removing or at least considerably reducing perhaps the single most important source of model dependence in the extraction of spectroscopic information from reaction data, are still subject to the influence of the choice of distorting potentials and the degree of sophistication of the reaction model employed. They also both depend on the binding energy of the transferred particle E_B and for levels close to threshold this can be a source of large uncertainties if the value is not well known, through uncertainties in the energy of the level and/or the masses of the core and valence particles; see, for example, Ref. [9].

As stated above, the basic premise of the ANC rests on the peripherality of the reaction used to extract it, i.e., only the tail of the bound-state wave function is probed by the measured quantity, the differential cross section. Reactions induced by heavy ions therefore have much to recommend them in this context over the more commonly applied light ion transfer reactions such as (d, p), (p, d), $(d, {}^3\mathrm{He})$, etc., because they usually occur at somewhat larger impact parameters. Heavy ion reactions also offer greater flexibility in the levels probed because the choice of different beams enables the kinematic matching conditions to be tuned to match the levels of interest. To set against this, heavy ion reactions are more likely to involve multistep transfer paths, which means that the DWBA, commonly used to extract ANCs from light ion reaction data, will no longer be a suitable reaction theory. This will complicate the analysis to some extent and extra data, such as inelastic scattering angular distributions, will be necessary to control the inputs describing the multistep paths. Also, the projectilelike overlaps are reasonably well established for the more popular light ion reactions which may not be the case for the equivalent heavy ion reactions.

Nevertheless, given a reasonably complete data set and a system where the projectilelike overlaps are well determined by other means it should be possible reliably to extract an ANC from heavy ion transfer data. While this has previously been done (see, for example, Ref. [10]), the analysis has usually been limited to a DWBA treatment. It therefore seems worthwhile to investigate the influence of multistep paths on the value of the ANC obtained from heavy ion reaction data for a system that meets the criteria of a fairly complete data set and where the projectilelike overlaps have already been carefully determined for the reaction of interest.

Such a data set exists for the $^{11}\mathrm{B} + {}^{14}\mathrm{C}$ system at an incident $^{11}\mathrm{B}$ energy of 45 MeV [11,12]. While the goal of the original experiment was a measurement of the elastic and inelastic scattering it has proved possible to extract an angular distribution for the $^{14}\mathrm{C}(^{11}\mathrm{B}, {}^{12}\mathrm{C})\,{}^{13}\mathrm{B}$ proton pickup reaction over a reasonable angular range. Full details of the experiment are given in Refs. [11] and [12]. Because of the experimental conditions the proton pickup angular distribution could only be obtained from the measurement of the carbon recoils and the peak corresponding to the $^{14}\mathrm{C}(^{11}\mathrm{B}, {}^{12}\mathrm{C})\,{}^{13}\mathrm{B}_{\mathrm{g.s}}$ reaction was kinematically resolved from the peak of the $^{14}\mathrm{C}(^{11}\mathrm{B}, {}^{14}\mathrm{C})\,{}^{11}\mathrm{B}_{4.44}$ inelastic scattering for $\theta_{\mathrm{lab}} > 17^\circ$ and the peak of the $^{14}\mathrm{C}(^{11}\mathrm{B}, {}^{14}\mathrm{C})\,{}^{11}\mathrm{B}_{2.12}$ inelastic scattering for $\theta_{\mathrm{lab}} < 37^\circ$. The angular distribution for the $^{14}\mathrm{C}(^{11}\mathrm{B}, {}^{12}\mathrm{C})\,{}^{13}\mathrm{B}_{\mathrm{g.s}}$ reaction was thus determined for center-of-mass angles $35^\circ \leqslant \theta_{\mathrm{c.m.}} \leqslant 70^\circ$. Because the necessary $\langle {}^{12}\mathrm{C} \mid {}^{11}\mathrm{B} + p\rangle$ overlaps have been carefully determined from a consistent analysis of $(e, e'p)$ and $(d, {}^3\mathrm{He})$ data [13] these data provide an excellent opportunity to test the influence of multistep paths on the extraction of the ANC for the $\langle {}^{14}\mathrm{C} \mid {}^{13}\mathrm{B} + p\rangle$ overlap from heavy ion reaction data. In addition, an extensive set of ANCs for both proton and neutron removal from p-shell nuclei was calculated [14] using the source term approach (STA) and compared with available empirical determinations, enabling the comparison of our result with a wide ranging systematics for similar systems.

II. DATA ANALYSIS

All reaction calculations described in this section were performed with the code FRESCO [15] and all parameter searches were carried out with the SFRESCO package.

A. Coupled channel analysis of the $^{11}\mathrm{B} + {}^{14}\mathrm{C}$ elastic and inelastic scattering

The first step was to fit the elastic and inelastic scattering data of Ref. [12] with a coupled channel (CC) calculation. Data included in the fitting procedure were the elastic scattering and inelastic scattering to the 2.125-MeV $1/2^-_1$, 4.445-MeV $5/2^-_1$, and 5.020-MeV $3/2^-_2$ levels of $^{11}\mathrm{B}$. Reorientation couplings were included for the 0.0-MeV $3/2^-_1$ and 4.445-MeV $5/2^-_1$ levels, the other two being considered as vibrational states. The 0.0-MeV $3/2^-_1$ Coulomb reorientation strength was fixed using the measured quadrupole moment of

TABLE I. Best-fit optical potential parameters for the 45-MeV $^{11}B + ^{14}C$ CC calculation. Both real and imaginary parts are of Woods-Saxon volume form, with radii given by $R_x = r_x(A_p^{1/3} + A_t^{1/3})$ fm. The Coulomb potential was of the standard form with radius parameter $r_C = 1.25$ fm.

V (MeV)	r_V (fm)	a_V (fm)	W (MeV)	r_W (fm)	a_W (fm)
197.0	0.774	0.801	4.99	1.437	0.770

this level [16] assuming the rotational model and $K = 3/2$. The 0.0-MeV $3/2^-_1 \rightarrow 5/2^-_1$ Coulomb coupling strength was fixed using the measured $B(E2)$ for this transition [17] and the corresponding reorientation coupling strength obtained assuming the rotational model (this state is considered to form part of a $K = 3/2$ rotational band built on the $3/2^-$ ground state). The 2.125-MeV $1/2^-$ level was treated as a single quadrupole phonon following Ref. [18] and the Coulomb coupling strength fixed using the measured $B(E2; 3/2^- \rightarrow 1/2^-)$ [19]. The 5.020-MeV $3/2^-_2$ level is weakly excited directly from the ground state by an $E2$ transition and much more strongly excited from the 2.125-MeV $1/2^-$ level. The Coulomb coupling strengths for both these transitions were also fixed using the measured $B(E2)$ values [17].

The initial optical potential parameters were taken from Ref. [12], set C. The nuclear coupling strengths for the inelastic excitations, i.e., the nuclear deformation lengths, and the optical potential parameters were then varied using the SFRESCO search package to obtain the best fit to the whole elastic and inelastic scattering data set. Two exceptions to this fitting procedure were the nuclear coupling strengths for reorientation of the 0.0-MeV $3/2^-_1$ and 4.445-MeV $5/2^-$ levels. The nuclear reorientation strength for the ground state was fixed to be in the same ratio to the $3/2^-_1 \rightarrow 5/2^-_1$ nuclear coupling strength as the respective Coulomb coupling strengths, and that for the 4.445-MeV $5/2^-$ level was fixed according to the rotational model. The resulting optical potential parameters are given in Table I and the nuclear deformation lengths in Table II. Note that in Table II the *reduced* deformation lengths are given, according to the convention given in the FRESCO manual [15]. In this way the coupling strengths are independent of any assumed value of K—essential here for those levels considered to be vibrational—although the values

TABLE II. Nuclear *reduced* deformation lengths obtained from the CC fit to the 45 MeV $^{11}B + ^{14}C$ elastic and inelastic scattering data.

Transition	δ (fm)
$3/2^-_1 \rightarrow 3/2^-_1$	0.894
$3/2^-_1 \rightarrow 5/2^-_1$	1.147
$5/2^-_1 \rightarrow 5/2^-_1$	−0.234
$3/2^-_1 \rightarrow 1/2^-_1$	0.894
$3/2^-_1 \rightarrow 3/2^-_2$	0.800
$1/2^-_1 \rightarrow 3/2^-_2$	2.000

TABLE III. ANC^2 values for the $\langle ^{12}C \mid ^{11}B + p\rangle$ overlaps calculated from the form factors of Kramer *et al.* [13] as used in this work. The theoretical values calculated using the STA [14] are also given.

A	A − 1	ANC^2 [13]	ANC^2 [14]
$^{12}C(0^+)$	$^{11}B(3/2^-_1)$	217.5	199
$^{12}C(0^+)$	$^{11}B(1/2^-_1)$	85.58	104
$^{12}C(0^+)$	$^{11}B(3/2^-_2)$	46.22	112

for transitions involving the $3/2^-_1$ and $5/2^-_1$ levels are consistent with their assumed status as members of a $K = 3/2$ rotational band.

B. Coupled reaction channels analysis of the $^{14}C(^{11}B, ^{12}C)\,^{13}B$ proton pickup

The next step was to include coupling to the $^{14}C(^{11}B, ^{12}C)\,^{13}B$ single proton pickup reaction in the analysis by means of the coupled reaction channels (CRC) method. Transfer paths including pickup with the ^{11}B core in its $3/2^-$ ground state and 2.125-MeV $1/2^-$ and 5.020-MeV $3/2^-_2$ excited states were included. The $\langle ^{12}C \mid ^{11}B + p\rangle$ overlaps were taken from the consistent analysis of $(e, e'p)$ and $(d, ^3He)$ data by Kramer *et al.* [13]. The corresponding ANC^2 values are listed in Table III together with the theoretical values of Ref. [14], calculated using the STA. The STA values are in reasonable agreement with the empirical values of Kramer *et al.* except for the $\langle ^{12}C(0^+) \mid ^{11}B(3/2^-_2)\rangle$ overlap where the STA value is more than a factor of two greater than the empirical one. The $\langle ^{14}C \mid ^{13}B + p\rangle$ overlap was determined by fitting the pickup data. To explore the variation of both the spectroscopic factor and the ANC for the $\langle ^{14}C \mid ^{13}B + p\rangle$ overlap as a function of the $p + ^{13}B$ binding potential, calculations were performed for a range of Woods-Saxon potentials with a fixed diffuseness $a_0 = 0.65$ fm and a radius parameter which was varied from $r_0 = 1.25$ to $r_0 = 1.75$ in steps of 0.1 fm. A Thomas form spin-orbit potential of fixed depth $V_{so} = 6$ MeV was also included, the depth of the central potential being adjusted to yield the correct proton binding energy. For each value of r_0 the best-fit spectroscopic factor and, hence, ANC value, was obtained by minimizing χ^2 for the fit to the proton pickup data, the coupling effect of the transfer paths on the elastic and inelastic scattering being minimal. Because CRC calculations require spectroscopic *amplitudes*, which are signed, whereas the overlaps of Kramer *et al.* only quote the spectroscopic factors (C^2S, the squares of the spectroscopic amplitudes), we fixed the necessary signs according to the results of the translationally invariant shell model calculations given in Ref. [12].

No suitable elastic scattering data are available for the $^{12}C + ^{13}B$ exit channel so a set of optical potential parameters obtained from a fit to the entrance channel elastic scattering at forward angles ($\theta_{c.m.} < 80^\circ$) was used, because the center-of-mass energy of the exit channel system is similar to that of the entrance channel in this case. The parameters were calculated according to a global optical potential for ^9Be, found to give

a reasonable description of ^{11}B elastic scattering [20]. An excellent description of the forward angle $^{11}\mathrm{B} + ^{14}\mathrm{C}$ elastic scattering was obtained by increasing the real potential radius parameter from 1.263 fm to 1.631 fm, all other parameters being as per the systematics of Ref. [20].

Calculations were performed both with and without ground-state reorientation of the ^{13}B included in the exit channel. The ground-state quadrupole moment of ^{13}B is similar to that of ^{11}B, being slightly smaller [21]. This was used to fix the Coulomb reorientation strength. The nuclear reorientation strength for ^{13}B was fixed using that obtained for ^{11}B and given in Table II and assuming that the nuclear deformation parameters β_N scale in the same ratio as the Coulomb ones, derived from the respective quadrupole moments assuming charge radii of $1.2A^{1/3}$ fm. This procedure resulted in a nuclear reduced deformation length of 0.846 fm for the ^{13}B ground-state reorientation coupling. Because the addition of the ground-state reorientation coupling of ^{11}B did not significantly alter the fit to the entrance channel elastic scattering data for angles $\theta_{\mathrm{c.m.}} < 80^\circ$ the same optical potential parameters were used in the exit channel for the calculations with and without ^{13}B reorientation coupling.

All calculations were performed using the prior form and included the full complex remnant term and nonorthogonality correction.

III. RESULTS

In Figs. 1 and 2 we compare the result of a typical CRC calculation—that with a proton binding potential radius $r_0 = 1.55$ fm and with ^{13}B reorientation coupling included in the exit channel—with the elastic and inelastic scattering and proton pickup data. The overall fit to the elastic and inelastic scattering data is good, the inelastic scattering to the 4.445-MeV $5/2^-$ level being the worst described. The proton pickup data are well described for angles $\theta_{\mathrm{c.m.}} < 55^\circ$, although the oscillations in the calculated angular distribution are somewhat more pronounced than those in the measured one, the calculated angular distribution falling off somewhat more rapidly with angle than the data beyond this point. Calculations with different proton binding potential radii gave almost identical descriptions of the data, as did calculations omitting the ^{13}B ground-state reorientation coupling in the exit channel, although the spectroscopic factors and ANCs obtained were different.

In Fig. 3 we plot the ANC^2 and C^{2}S values obtained from the CRC analyses with and without ^{13}B ground-state reorientation coupling in the exit channel as a function of the proton binding potential radius r_0. The error bars represent the ranges giving χ^2 values for the fit to the proton pickup data up to 10% larger than the minimum in each case. The solid curves denote regression fits with quadratic functions of r_0. It is immediately apparent from the figure that both the spectroscopic factor and the ANC^2 vary to a high degree of accuracy as quadratic functions of the proton binding potential radius r_0. As expected, there is a significant variation in C^{2}S as r_0 is increased from 1.25 to 1.75 fm. By contrast, the corresponding variation in the ANC^2, while not negligible, is not significant within the quoted uncertainties. This is in accord with the

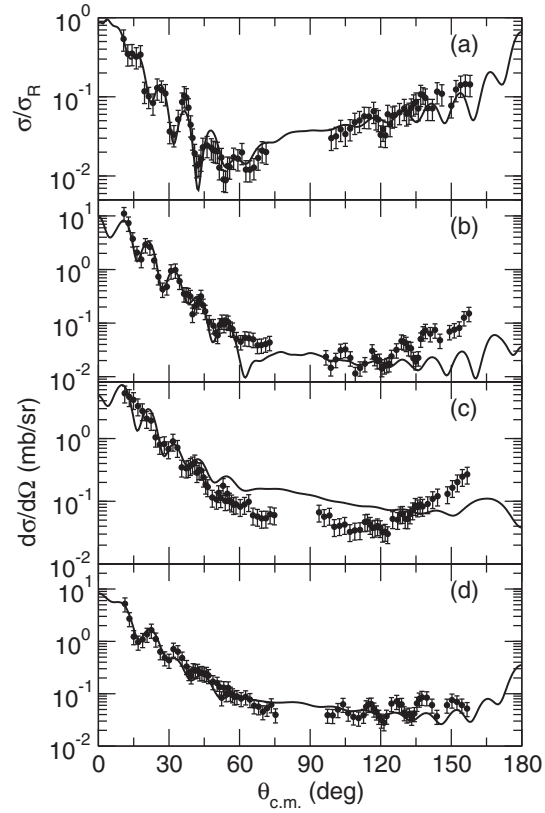

FIG. 1. CRC fit to the 45-MeV $^{11}\mathrm{B} + ^{14}\mathrm{C}$ elastic scattering (a) and inelastic scattering to the 2.125-MeV $1/2^-$ (b), 4.445-MeV $5/2^-$ (c), and 5.020-MeV $3/2^-_2$ (d) levels of ^{11}B. The proton binding potential radius $r_0 = 1.55$ fm and ^{13}B reorientation coupling was included in the exit channel.

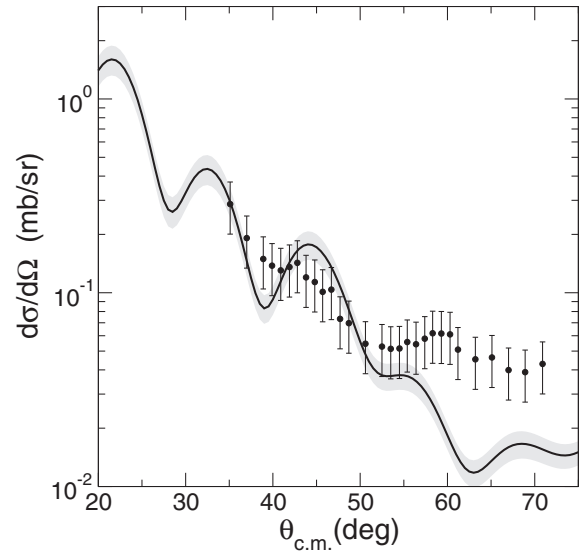

FIG. 2. CRC fit to the 45-MeV $^{14}\mathrm{C}(^{11}\mathrm{B}, ^{12}\mathrm{C})\,^{13}\mathrm{B}$ single proton pickup data. The proton binding potential radius $r_0 = 1.55$ fm and ^{13}B reorientation coupling was included in the exit channel. The shaded area denotes the effect of changing the spectroscopic factor to give a 10% increase in χ^2 from the minimum value.

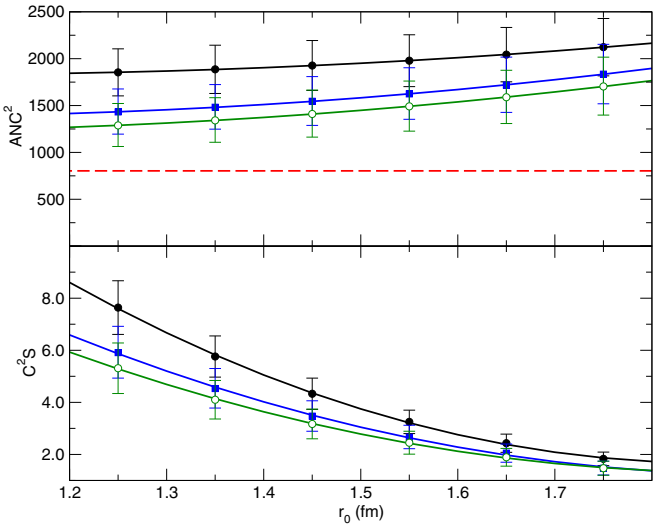

FIG. 3. Best-fit ANC^2 and C^{2}S values for calculations describing the 45-MeV ^{14}C(^{11}B, ^{12}C) ^{13}B single proton pickup data as a function of the proton binding potential radius r_0. The open circles are the results of CRC calculations including ^{13}B ground-state reorientation coupling in the exit channel, the filled squares CRC calculations without the ^{13}B reorientation, and the filled circles DWBA calculations. The solid curves are regression fits with quadratic functions of r_0. The dashed line denotes the $\langle ^{14}\mathrm{C} \mid ^{13}\mathrm{B} + p\rangle$ ANC^2 value of Ref. [14].

usual expectation that the ANC is less dependent on the exact form of the bound-state radial wave function, because it is the normalization of the asymptotic tail of the overlap function.

While the uncertainties are such that the difference in the ANC^2 (and spectroscopic factor) for the calculations with and without ^{13}B ground-state reorientation coupling in the exit channel are not significant the inclusion of the reorientation coupling does lead to a systematically lower value of the ANC^2 for a given value of r_0. This suggests that the degree of sophistication in modeling the reaction mechanism could have an influence on the extracted ANC that needs to be taken into account. As a further probe of this possibility we also performed similar sets of DWBA calculations, an approach often used in studies of this kind. These employed the modified global parameters of Ref. [20] in both entrance and exit channels, i.e., the entrance channel elastic scattering was only described for angles $\theta_{\mathrm{c.m.}} < 80^\circ$. The other inputs were similar to those of the CRC calculations described in the previous section. The resulting ANC^2 and C^{2}S values are plotted on Fig. 3 as the filled circles. They also vary as a quadratic function of r_0 and show a significant increase over the values obtained from either CRC analysis.

The theoretical maximum value of C^{2}S for pickup from a full $p_{3/2}$ shell is 4.0 according to the convention used in the FRESCO code. If we therefore rule out the results that yield C^{2}S > 4.0 as unphysical and take the error weighted mean we arrive at the values for the ANC^2 for the three sets of calculations given in Table IV. Also given in Table IV is the theoretical value of Ref. [14], calculated using the STA. Two things are apparent: first, the DWBA result is significantly larger than either of the CRC determinations, and secondly,

TABLE IV. Error weighted mean ANC^2 values obtained from the CRC calculations with and without ^{13}B ground-state reorientation coupling in the exit channel and the DWBA calculation. Note that results corresponding to a value of C^{2}S > 4.0 were omitted from the determination of the mean values.

Source	ANC^2 (fm^{-1})
DWBA	2044 ± 168
CRC (no ^{13}B reor)	1716 ± 170
CRC (^{13}B reor)	1532 ± 138
Theoretical (STA) [14]	803

the lowest empirical value obtained here, that from the CRC calculation including ^{13}B ground-state reorientation coupling in the exit channel, is still approximately twice the STA value.

IV. SUMMARY AND CONCLUSIONS

The availability of a comparatively complete data set for the elastic and inelastic scattering of ^{11}B from a ^{14}C target [11,12], plus the data for the ^{14}C(^{11}B, ^{12}C) ^{13}B proton pickup reaction presented here, has enabled the extraction of an empirical value for the $\langle ^{14}\mathrm{C} \mid ^{13}\mathrm{B} + p\rangle$ ANC. While, as expected, for a set of calculations using the same model of the reaction mechanism the ANC was not sensitive within the estimated uncertainties to the proton binding potential radius over a wide range, the value obtained did depend on the choice of reaction model/coupling scheme. The use of the DWBA compared to a more complete CRC coupling scheme led to a significantly larger value for the ANC, and even within the CRC formalism the exact choice of coupling scheme was found to have a systematic effect on the value obtained for the ANC, although in the particular cases explored here this was not significant within the uncertainties.

Both the ANC and the spectroscopic factor were found to vary as quadratic functions of r_0, the proton binding potential radius parameter, the spectroscopic factor being much more sensitive to the choice of r_0, as expected. Because under the convention adopted by the reaction code used to analyze the data, FRESCO [15], the theoretical maximum value of the spectroscopic factor for pickup of a nucleon from a filled shell is $(2j + 1)$, ANCs for values of r_0 corresponding to spectroscopic factors C^{2}S > 4.0 were eliminated from the final determination. The error weighted mean value for the ANC^2 obtained from this analysis, 1532 ± 138 fm^{-1}, is approximately a factor of two larger than that calculated using the STA, 803 fm^{-1} [14]. This ratio is consistent with those for proton removal from ^{11}C, ^{13}N, and ^{13}O plotted on Fig. 2 of Ref. [14], although the uncertainty in the experimental value for ^{13}O is large.

Analysis of the data using the DWBA instead of the CRC formalism yielded a significantly larger ANC, indicating sensitivity to the modeling of the reaction process. The influence of different possible reaction paths must therefore at least be checked in analyses of this kind if reliable ANC values are to be obtained. Our conclusion is that heavy ion reactions can form a useful alternative to the more traditional light ion

reactions as a means to extract structure information, provided that a reasonably complete data set is available so that different possible reaction paths may be included realistically and that the necessary "opposing" overlaps (in this case the $\langle^{12}\mathrm{C} \mid {}^{11}\mathrm{B} + p\rangle$) have already been determined with sufficient precision.

[1] M. Dost and W. R. Hering, Z. Naturforsh. **21**, 1015 (1966).
[2] P. J. A. Buttle and L. J. B. Goldfarb, Nucl. Phys. **78**, 409 (1966).
[3] J. Rapaport and A. K. Kerman, Nucl. Phys. A **119**, 641 (1968).
[4] A. Strömich, B. Steinmetz, R. Bangert, B. Gonsior, M. Roth, and P. von Brentano, Phys. Rev. C **16**, 2193 (1977).
[5] L. D. Blokhintsev, I. Borbely, and E. I. Dolinskii, Fiz. Elem. Chastits At. Yadra **8**, 1189 (1977); Sov. J. Part. Nuclei **8**, 485 (1977).
[6] L. D. Blokhintsev, A. M. Mukhamedzhanov, and A. N. Safronov, Fiz. Elem. Chastits At. Yadra **15**, 1296 (1984); Sov. J. Part. Nuclei **15**, 580 (1984)
[7] A. M. Mukhamedzhanov and R. E. Tribble, Phys. Rev. C **59**, 3418 (1999).
[8] A. M. Mukhamedzhanov, Phys. Rev. C **86**, 044615 (2012).
[9] N. Keeley, K. W. Kemper, and K. Rusek, Eur. Phys. J. A **54**, 71 (2018).
[10] X. Tang, A. Azhari, C. Fu, C. A. Gagliardi, A. M. Mukhamedzhanov, F. Pirlepesov, L. Trache, R. E. Tribble, V. Burjan, V. Kroha, F. Carstoiu, and B. F. Irgaziev, Phys. Rev. C **69**, 055807 (2004).
[11] S. Yu. Mezhevych, K. Rusek, A. T. Rudchik, A. Budzanowski, V. K. Chernievsky, B. Czech, J. Choiński, L. Głowacka, S. Kliczewski, E. I. Koshchy, V. M. Kyryanchuk, A. V. Mokhnach, A. A. Rudchik, S. B. Sakuta, R. Siudak, I. Skwirczyńska, A. Szczurek, and L. Zemło, Nucl. Phys. A **724**, 29 (2003).
[12] S. Yu. Mezhevych, A. T. Rudchik, K. Rusek, K. W. Kemper, S. Kliczewski, E. I. Koshchy, A. A. Rudchik, S. B. Sakuta, J. Choiński, B. Czech, R. Siudak, and A. Szczurek, Eur. Phys. J. A **50**, 4 (2014).
[13] G. J. Kramer, H. P. Blok, and L. Lapikás, Nucl. Phys. A **679**, 267 (2001).
[14] N. K. Timofeyuk, Phys. Rev. C **88**, 044315 (2013).
[15] I. J. Thompson, Comput. Phys. Rep. **7**, 167 (1988).
[16] R. K. Nesbet, Phys. Rev. Lett. **24**, 1155 (1970).
[17] J. H. Kelley, E. Kwan, J. E. Purcell, C. G. Sheu, and H. R. Weller, Nucl. Phys. A **880**, 88 (2012).
[18] V. Hnizdo, C. W. Glover, and K. W. Kemper, Phys. Rev. C **23**, 236 (1981).
[19] M. P. Fewell, R. H. Spear, T. H. Zabel, and A. M. Baxter, Aust. J. Phys. **33**, 505 (1980); **37**, 239 (1984).
[20] Y.-L. Xu, Y.-L. Han, H.-Y. Liang, Z.-D. Wu, H.-R. Guo, and C.-H. Cai, Chin. Phys. C **44**, 034101 (2020).
[21] T. Nagatomo *et al.*, Hyperfine Interact. **159**, 269 (2004).